RESEARCH

Semi-real time systems for subsidence monitoring in areas affected by underground mining: the example of the Nuraxi-Figus coal district (Sardinia, Italy)

L. Ammirati[1] · D. Di Martire[1] · F. Bordicchia[3] · D. Calcaterra[1] · G. Russo[1] · N. Mondillo[1,2]

Abstract

Underground mining can produce subsidence, which can be coincident with mining activities or delayed in response to the time-dependent deformation of the rocks. Therefore, in these cases, it is essential to effectively monitor the soil deformations at different times during and after mining activity. In the present work, an integrated approach based on geotechnical numerical modeling and Advanced Differential Interferometric Synthetic Aperture Radar (A-DInSAR) method has been applied to detect, study and monitor the subsidence related to mining activity in the Nuraxi Figus coal district (Sardinia, Italy). Two datasets of high-resolution COSMO-Skymed images were acquired, respectively in two covering periods: from 2011 and 2014, and from 2013 to 2020. The A-DInSAR results show that the predominant displacement rates are located in correspondence with the panels. The cumulated satellite-based LoS displacements vary in the first period between -130 and $+28$ mm and -293 and $+28.4$ mm, while, during the second period between -6.9 and $+1.6$ mm and -8.72 and $+4.33$ mm in ascending and descending geometries, respectively. The geotechnical numerical model allowed to obtain a value for the maximum expected. By using the vertical and horizontal components it was possible to reconstruct the kinematics of the deformation considering three phases: pre-mining, syn-mining, and post-mining activity. The temporal evolution of displacements started during the mining extraction in 2011, achieved the major values in correspondence of post-mining operations, during the period from 2013 to 2014 and continued slowly until 2020. The near real-time monitoring system applied in this study proved to be very useful for detecting subsidence during the mining activity and the post-mining period.

Keywords Mining monitoring · A-DInSAR · Numerical modeling · Subsidence · Underground mining

1 Introduction

Mining and mineral extraction is useful for human development, social progression, and material prosperity. However, these activities strongly interact with surrounding environments and could produce meaningful negative effects, on the atmosphere, soil, and water (Bell et al. 2000). One of the main issues in many parts of the world is represented by the subsidence induced by underground mining (Villegas et al. 2011; Zhou et al. 2015; Przyłucka et al. 2015a, b; Vu Khac et al. 2021). Such effects are more harmful when the activities legal or not authorized are in correspondence or nearby urban areas (Bell et al. 2005; Prakash et al. 2010; Ji et al. 2011; Villegas et al. 2011; Marschalko et al. 2012). Subsidence can either coincide with mining activities or be delayed in response to the time-dependent deformation of rocks. Several studies determined the rate of expected subsidence employing physical or numerical modeling and analysis (Whittaker 1989; Singh et al. 1998; Alheib et al. 2001; Ye et al. 2016; Xie et al. 2020; Gazzola et al. 2021). In any case, to avoid possible environmental harm it is important to monitor areas subjected to underground mining activity. Mining-related subsidence is usually analyzed either by in-situ measurements, or by aerial photographs on specific sites (Armenakis 1983). As far as in-situ survey techniques concerns, they consist of: piezometers, useful to register

✉ D. Di Martire
   diego.dimartire@unina.it

[1] Department of Earth Sciences, Environment and Resources, University of Naples, Federico II, 80126 Naples, Italy

[2] Department of Earth Sciences, Natural History Museum, London SW7 5BD, UK

[3] Sardinia Region Company Carbosulcis S.P.A., 09010 Gonnesa, CI, Italy

pore pressure variations of the overburden strata (Guo et al. 2012); extensometers installed at different heights in boreholes located above the exploited panels: in this way, settlments are measured (Holla et al. 2000); and GNSS technique with benefits of accuracy and simultaneous 3-D positioning (Chen et al. 2014). However, these techniques are tedious and time-consuming, with small area coverage. Indeed, they have a cost of implementation that is significantly expensive for the management and the acquisition of information on large spatial and temporal scales of the entire mining area, thus providing localised and not distributed results.

Due to these limitations, remote sensing can be a cost-effective technique. Specifically, among the different types of remote sensing techniques, the Advanced Differential Interferometric Synthetic Aperture Radar (A-DInSAR—Franceschetti et al. 1992) proved to be a very powerful tool, being sensitive to sub-centimetric ground movements (Colesanti et al. 2006) and/or terrain displacements, induced by landslides (Wasowski and Bovenga 2022; Scifoni et al. 2016; Pappalardo et al. 2018; Giardina et al. 2019; Guerriero et al. 2019), earthquakes (De Novellis et al. 2018; Zhao et al. 2021), volcanoes (Foumelis et al. 2016; Casu et al. 2019) and valid to detect harm to structures and infrastructures (Milillo et al. 2018; Ullo et al. 2019; Pastor et al. 2019; Miano et al. 2021). In the last three decades, A-DInSAR has been applied also in mining areas to detect subsidence due to underground activity (Yue et al. 2011; Du et al. 2016; Ammirati et al. 2020; Pawluszek et al. 2020; Chen et al. 2021), monitoring the stability of tailings dam (Necsoiu et al. 2015; Gama et al. 2019; Ammirati et al. 2021), and to identify surface movements in open-pit mines (Paradella et al. 2015; Carlà et al. 2018). The scientific community has studied many cases of mining subsidence in coal districts (Salmi et al. 2017; Jing et al. 2018; Zingano et al. 2019). In these areas, A-DInSAR resulted to be an effective technique for ground movement surveys (Dong et al. 2013; Xu et al. 2020). In several studies, the subsidence maps generated from satellite images proved to be consistent with field observations (Ismaya et al. 2012; Samsonov et al. 2013; Pawluszek et al. 2020).

From this point of view, it is essential to not underestimate the potential effects of mining activities and constant monitoring the mineral resource exploitation and its effects on the ecological environment. Furthermore, mining monitoring is of greatest importance, not only for the scientific community but also for the mining companies, to reduce the potential effects and consequences.

In this work, an integrated approach based on geotechnical numerical modeling and A-DInSAR method was applied for investigating subsidence phenomena which occurred in a coal mining area affected by underground exploitation.

The innovativeness of this application lies in several aspects: (1) it is one of the first applications in the mining sector on Italian territory, (2) the time interval analyzed is about 10 years, thus allowing coverage of both the pre-, syn- and post-mining phases, (3) unlike previous works very high-resolution COSMO-SkyMed images were processed; in fact, there are few applications in the world that have used very high-resolution images for monitoring underground mining areas (Przyłucka et al. 2015a, b; Alam et al. 2022), finally, (4) it is one of the first combined applications, in the Italian mining sector, between a research institution and mining company with the objective of monitoring the rehabilitation of a dismissed mining area.

The study area is represented by a historic coal mining district located in southwest Sardinia, Italy, in the municipality of Nuraxi Figus (Carbonia-Iglesias province). The area occurs in the Carbosulcis S.p.A. mining concession called "Monte Sinni" (total extension of about 0.6 km^2), where a subsidence phenomenon occurred between the years 2011 to 2014 (Tessitore et al. 2018). In the present study, we analyzed the remote sensing data, obtained in the framework of Not-Ordinary Plan of Environmental Remote Sensing (Piano Straordinario di Telerilevamento Ambientale—in Italian), funded by the Italian Ministry of Environment (Costantini et al. 2017; Di Martire et al. 2016), to correlate the 2011–2014 subsidence phenomenon with the underground mining activity and the excavation development, also using numerical modeling to reconstruct the kinematic evolution of ground displacements. Moreover, radar satellite data, derived from COSMO-SkyMed (CSK) datasets, were carried out by SUBSIDENCE software, which implements the Coherent Pixels Technique algorithm (Mora et al. 2003; Iglesias et al. 2015), for the period from 2013 to 2020, to understand the temporal evolution of ground surface deformation. The study allowed us to understand the cause-effect mechanism between extraction and ground deformation and confirmed that ground surface deformations can continue at lower rates a few years after the completion of mining activities.

2 History of mining activity in the Sulcis coal basin

In the Sulcis coal district, the mining activity started around 1850 through the exploitation of productive coal outcrops occurring in the sedimentary rocks of the Lignitifero Formation (Fig. 1). During this period, coal became the primary national resource and was mostly exploited in open-pits (Fig. 2).

Since 1976, Carbosulcis S.p.A., which is the current owner of the mining licenses in the Sulcis district, started mining activity south of Seruci, in the Monte Sinni area, nearby the Nuraxi Figus village (Fadda et al. 1994). The Monte Sinni coal panels are located at a depth of about 400 m b.g.l., extend for an area of 55 km^2 and are mined
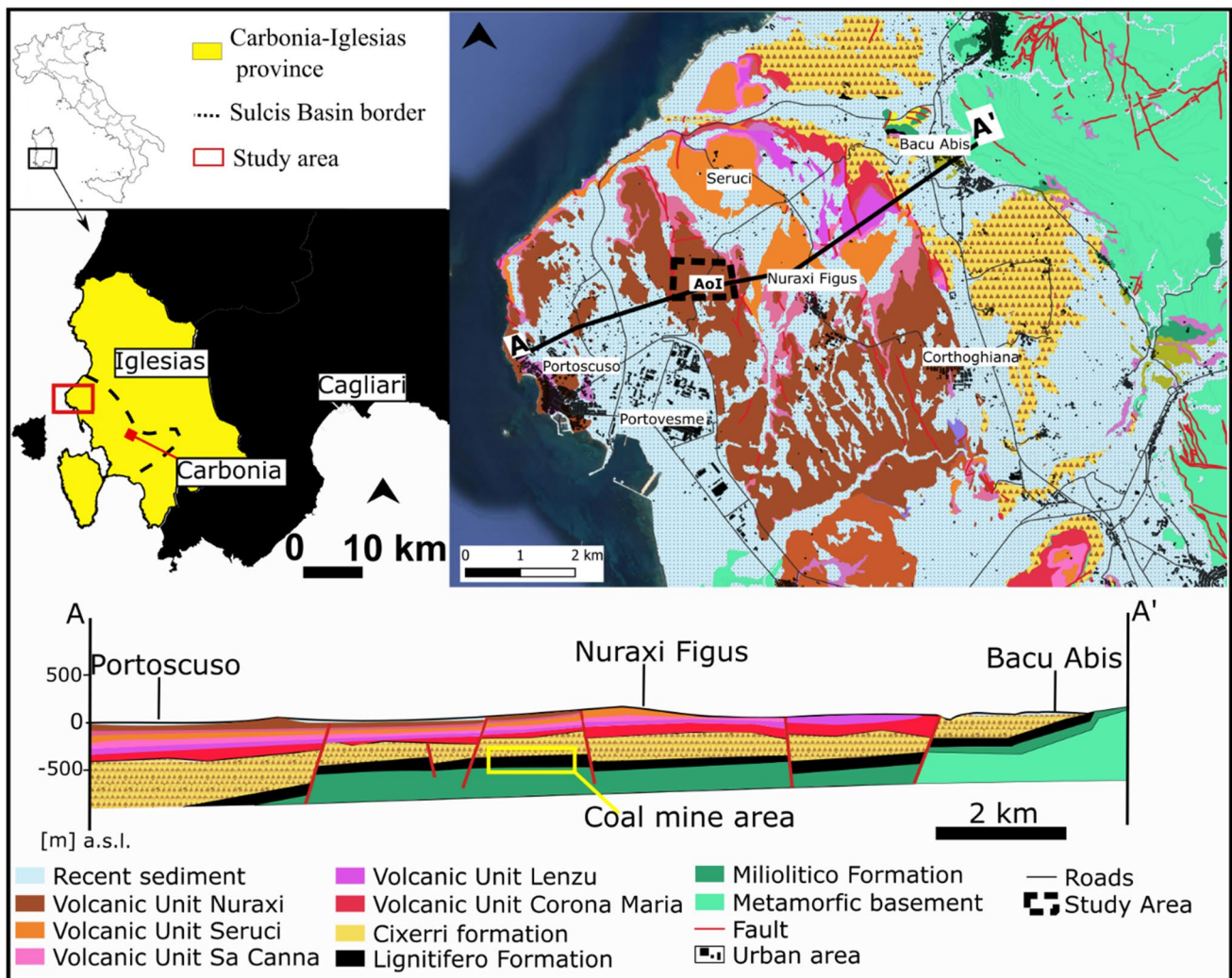
Fig. 1 Location map (left); Geological sketch map (right); The geological cross-section (below)

through 30 km of tunnels (15 km of which correspond to permanent infrastructures). Mining activity was conducted in correspondence with some exploitation panels, called W1, W2, W3, etc., with average dimensions of 300 m × 600 m (width × length) and a height of about 3 m (Fig. 3). In the initial period of activity, mining was developed through room and pillars method, whereas from the 1980s the coal extraction was carried out with a different method, called "longwall cutting in retreat". The latter is based on the continuous extraction of the coal panel through a shearer that digs along the coal face, while a transporter belt carries away the grained coal. When the shearer moves on, the roof of the gallery at the back of the active face collapses. The Carbosulcis S.p.A. used the longwall method to extract the W3 and W4 panels, in the periods between 2008 and 2010 and from 2011 to 2012, respectively. In 2018, following the progress of environmental regulations on the cessation of the use of coal, the

Company started the closure plan that progressively will bring to reclaim all the areas by 2027.

3 Geological and geotechnical features

Geology of the Sulcis district is characterized by Cenozoic sedimentary and volcanic rocks, unconformably overlaying a Paleozoic basement. The Cenozoic sedimentary rocks consist of limestones, sandstones, conglomerates, marls, and silty clays, and are formally subdivided into four stratigraphic formations. At the basis of the Cenozoic succession, the oldest rocks are represented by the limestones of the Macro-foraminifera Formation, which are covered by the sandstones, marls and limestones of the Miliolitico Formation (20–70 m thick; Lower Eocene age). The following stratigraphic interval is represented by clays, marly limestones, bituminous limestones, marls, and conglomerates of
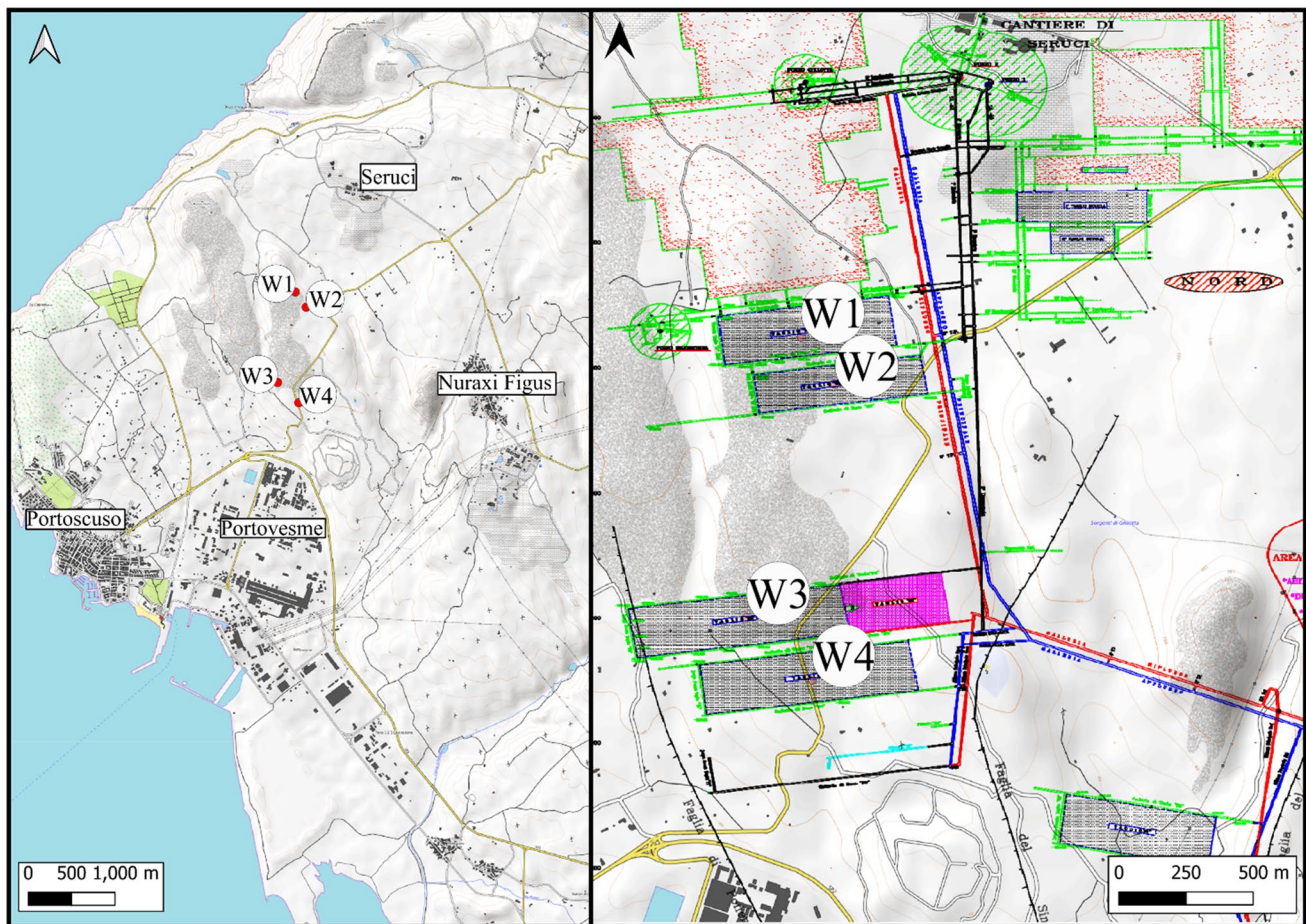
Fig. 2 Location of exploitation panels, W1, W2, W3, W4. On right the maps of underground tunnels and excavation areas

the Lignitifero Formation (70–150 m thick; Lower-Middle Eocene age). which hosts the coal horizons object of mining activity. Coal seams commonly are 10 cm thick, rarely reaching 30–50 cm, and are interbedded with clays (Assorgia et al. 1992a and b). The Lignitifero Formation is covered by about 300 m of sandstones, conglomerates, and marls of the Cixerri Formation (Eocene–Oligocene; Pasci et al. 2010). The whole Cenozoic sedimentary succession is in turn covered by volcanic rocks, represented by twelve andesitic, dacitic to rhyolitic ignimbrite plateaus belonging to several stages of explosive volcanic activity of Oligo-Miocene age (Morra et al. 1994). The whole district has been dislocated by normal faults, which lower the sedimentary succession to various hundred meters of depths within the basin (Barca et al. 2000). These geological features allow the existence in the area of two types of aquifers: one occurring in the volcanic rocks and a second one in the Miliolitico Formation, which have been both dewatered by Carbosulcis S.p.A. before the start of the underground mining activity.

From a geotechnical point of view, the Rock Mass Rating (RMR) (Bieniawski 1989) was used to numerically define the characteristics of the rocks, using "RMR value" for defining five quality classes (from very poor to very good). In particular, 89% of the volcanic rocks correspond to the fair class (III), whereas the sedimentary Formations are characterized by 57% to the fair class (III), 28% to the poor class (IV), and 10% to the good class (II) (Fadda et al. 1994). According to Fadda (1994) the Cixerri Formation has a heterogeneous structure, where conglomerate and marls layers belong to the lowest classes, while sandstones are characterized by the best performance.

4 Materials and methods

For the present study, as summarized in the flow chart of Fig. 3, satellite data and mining information were used to create a near-real time monitoring system. Satellite data were collected in ascending and descending geometries covering the time span 2011–2020, to study subsidence by the vertical deformation maps and the displacement time
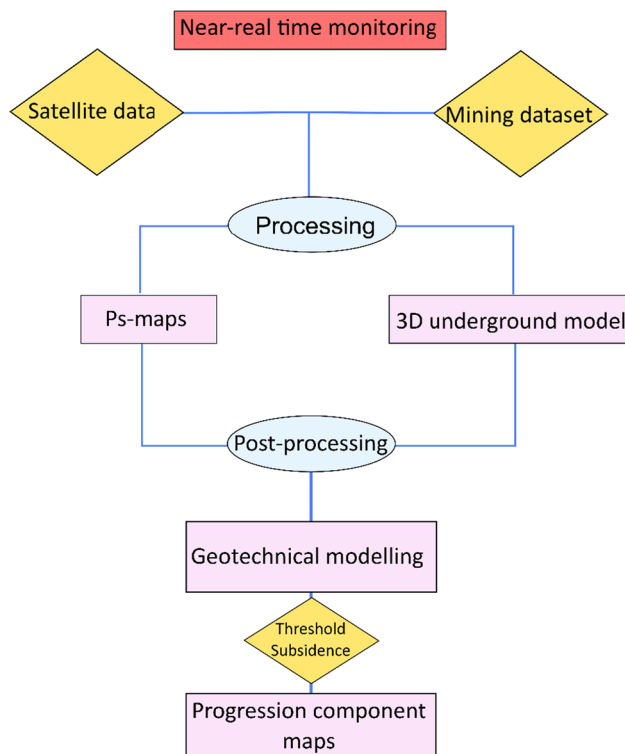
Fig. 3 Flow chart of the methodological approach

Fig. 4 Geometry acquisition: **a** Ascending; **b** Descending

series. Two datasets composed of high-resolution images have been used:

(1) Satellite data 1 (SD1): PSP-IFSAR algorithm (Costantini et al. 2008), time 2011–2014, obtained in the framework of Not-Ordinary Plan of Environmental Remote Sensing (Piano Straordinario di Telerilevamento Ambientale—in Italian), funded by the Italian Ministry of Environment (Costantini et al. 2017; Di Martire et al. 2017).

(2) Satellite data 2 (SD2): SUBSIDENCE software (Mora et al. 2003; Iglesias et al. 2015), covering the period 2013–2020.

SD1 consist of 41 images acquired in ascending geometry and 58 images acquired in descending geometry in the time interval May 2011–March 2014. SD2 contains 102 and 116 images in ascending and descending orbit, respectively related to the period from October 2013 to July 2020. First data set derived from the interferometric processing within the framework of the third stage of the PST-A project (Not-Ordinary Plan of Environmental Remote Sensing) funded by the Ministry for the Environment and Protection of the Territory and the Sea (Italian National Geoportal, www.pcn.minambiente.it). The second dataset was obtained by the processing of SD2 using SUBSIDENCE software, which implements the Coherent
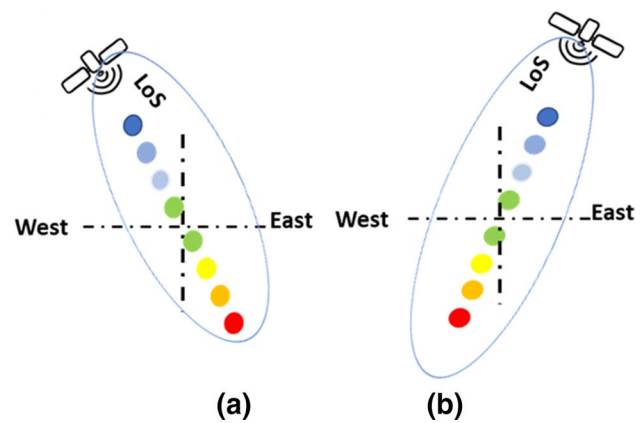
Pixels Technique (CPT) algorithm, developed at the Remote Sensing Laboratory (RSLab) of the Universitat Politecnica de Catalunya of Barcelona. SUBSIDENCE uses the CPT-Temporal Phase Coherence (CPT-TPC) approach to extract from a stack of differential interferograms the deformation evolution over wide areas during large periods (Mora et al. 2003; Iglesias et al. 2015). The processing is structured in three main phases:

(1) Interferogram generation: the generation of the best interferogram set among all the available images of the zone under study;

(2) The Stable Coherence Scatterers (SCS) selection: the points in the detected area characterized by signal stability and higher than the threshold in a specific percentage of interferograms. To get enough SCSs a coherence limit of 0.6 was considered, assuming an error in mean displacement rate lower than 1.5 mm;

(3) Linear velocity of deformation (Iglesias et al. 2015): linear deformation time series (TS) were calculated starting from phase analysis. The Delaunay triangulation was used to check an offset among the different interferograms. Then, it was applied a filtering process to assess the deformation evolution of selected pixels (SCS) (Blanco et al. 2008); the geocoding of the results was carried out in WGS84-UTM.

This process allowed to elaborate PS (Permanent Scatters) maps for each acquisition geometry in terms of mean displacement rate and time series of deformation, along the Line of Sight (LoS) of the satellite (Fig. 4). For a better understanding of the results, it is necessary to clarify the acquisition mode. Satellites move two semi-polar orbits defined as ascending and descending, moving from South to North and North to South, respectively, sending electromagnetic signals along the Line of Sight (LoS) to identify targets on the surface. By convention, displacements approaching from the sensor will take on positive values (blue), while displacements away the sensor will take on negative values (red—Fig. 4).

After this, by using images acquired in ascending and descending geometries the vertical displacement component was calculated (Cascini et al. 2010; Di Martire et al. 2013). Subsequently, to improve the analysis of the Nuraxi Figus subsidence, satellite datasets were integrated with the following information, provided by Carbosulcis S.p.A.: stratigraphic logs of 9 drillholes, geotechnical parameters of country rocks, mining reports regarding the exploitation of panels W3 and W4, and maps of underground tunnels and excavation areas. Spatial migration in time of the excavation front within the mining panels W3 and W4 was compared with the evolution of vertical ground displacements detected with the satellite data during the mining activity.

The 3D geological model of the subsurface was elaborated by using lithostratigraphic data from 7 boreholes through the software Rockworks® (Fig. 5).

The model allowed us to determine the thickness of the overburden strata in the various parts of the study area. A stratigraphic section perpendicular to the W3 and W4 exploitation panels was extracted from the 3D geological model to produce a numerical subsoil model through the Plaxis® 2D software (Brinkgreve et al. 2008). The finite element numerical model allowed us to model the excavation process in two-dimensions in order to quantify the subsidence induced at surface level. The characteristic values of geotechnical rock parameters used for modelling (Table 1) were obtained by Carbosulcis S.p.A.

As reported in Table 1, due to similar geotechnical parameters, the twelve ignimbrite plateaus overlying the

Table 1 Geotechnical parameters used for modeling. The volcano-pyroclastic rocks and ignimbrites are named Volcanic 1 to 4. The Cixerri Fm. is subdivided into two patterns. Retrieved from Carbosulcis S.p.A

Geology layer	Unit weight γ (kN/m^3)	Young's modulus E (N/m^2)	Poisson's ratio v
Volcanic 1	22	2.60×10^7	0.25
Volcanic 2	14	1.94×10^6	0.25
Volcanic 3	22	2.00×10^7	0.21
Volcanic 4	23	1.06×10^7	0.12
Conglomeratic Cixerri Fm	22	1.00×10^6	0.40
Cixerri Fm	24	9.00×10^6	0.30
Lignitifero Fm	13	1.00×10^5	0.28
Miliolitico Fm	26	1.50×10^{10}	0.30

sedimentary units were grouped in four geotechnical layers. Cross sections (width = 200 m, height = 3 m) of panels W3 and W4 were considered in the 2D model at the depth of 400 m. Each rock layer has been considered in the numerical model as linear elastic, with Young modulus E and Poisson's ratio n as reported in Table 1. Evaluation of the overall subsidence (total vertical displacements of the surface) has been performed at the end of the following calculation steps: (1) initial in situ stresses (geostatic stresses), (2) excavation of W4 panel, and (3) excavation of W3 panel.
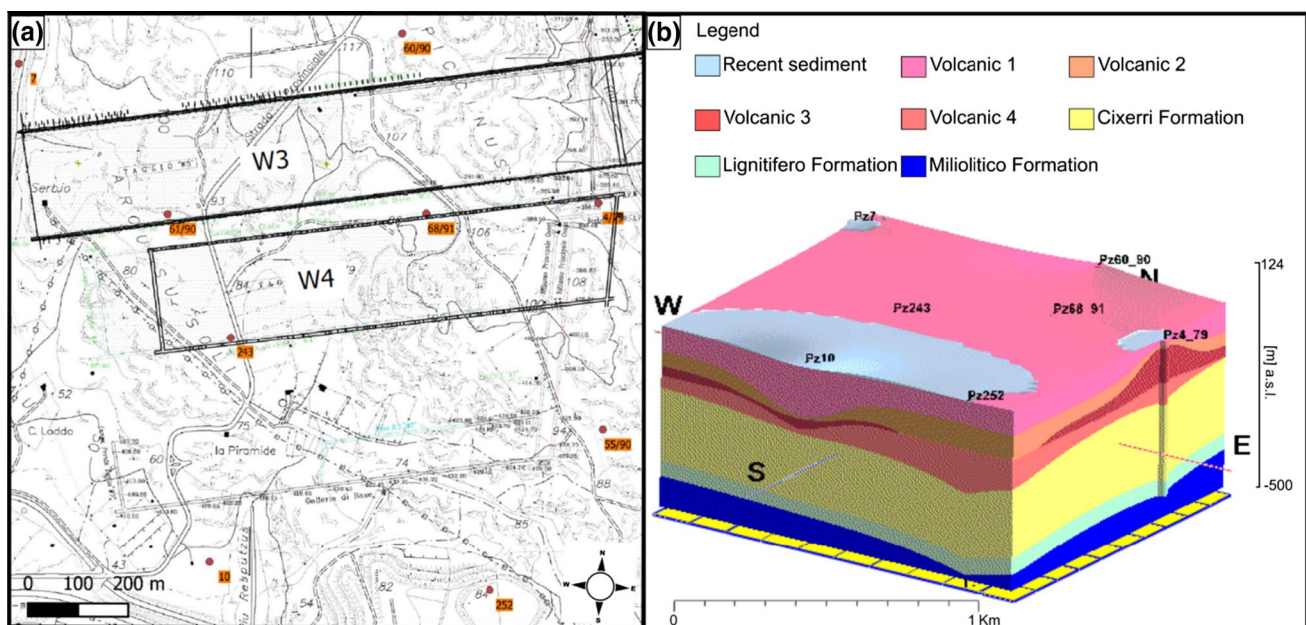

Fig. 5 **a** Location of stratigraphic logs used to elaborate **b** 3D geological model of subsurface

5 Results

5.1 Processing phase

Starting from two satellite datasets, four PS-displacement rate maps for both acquisition geometries (ascending, descending) have been created. The PSs obtained were imported into GIS platform and subsequently made visible according to a colour scale: negative values conventionally indicate a movement of the target away from the satellite (LoS), while positive values indicate movement towards the sensor; stable areas are shown by using the green color (see Fig. 4). The maps represent the average velocity recorded during the period covered by the acquisitions (Fig. 6). The results of both ascending and descending geometries show that the predominant displacement rates are located in correspondence with the panels.

In the central part of the monitored area, in the first period considered (2011–2014), PS-deformation velocities exceed the detection limits (Colesanti et al. 2006), and no satellite-based measurements are available. On the contrary, in the second period analyzed (2013–2020), the same zone is covered by PS-measurements.

This fact is likely related to the decrease in displacement velocities. Indeed, the cumulated satellite-based LoS displacements vary between -130 and $+28$ mm (until January 2014), -293 and $+28.4$ mm (until March 2014) and between -6.9 and $+1.6$ mm (until March 2020), -8.72 and $+4.33$ mm (until March 2020) in ascending and descending geometries, respectively. In the 3D subsurface geological model of the investigated area (Fig. 5), it is possible to see the position of the Lignitifero Formation, which hosts the mined horizon at 350–500 m b.g.l. The thickest rock layers overlying this interval correspond to the sandstones and conglomerates of the Cixerri Formation. The volcano-pyroclastic rocks and ignimbrites (named Volcanic 1 to 4) have a thickness that varies from 100 to 298 m.
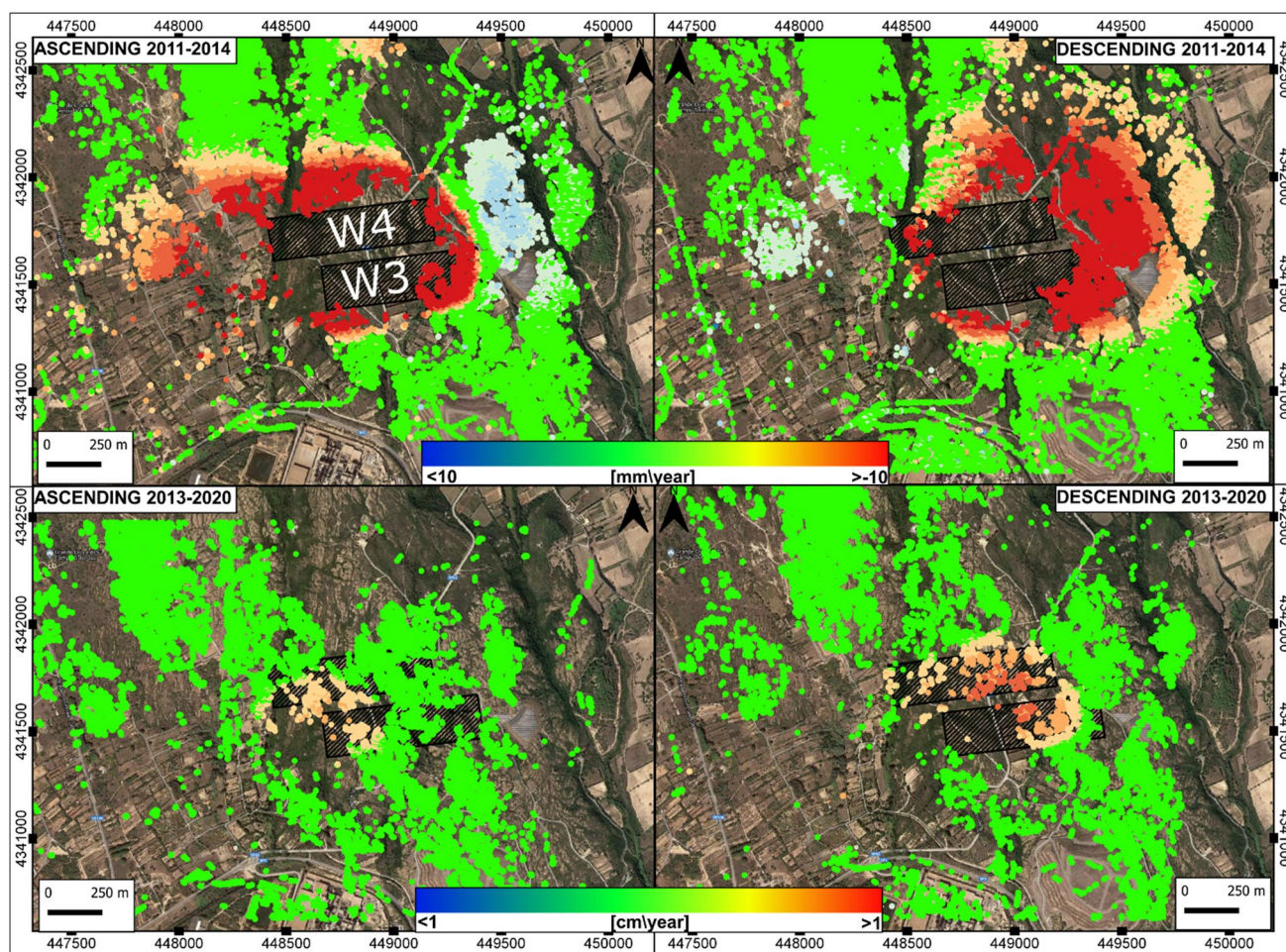

Fig. 6 Mean displacement rate maps in ascending and descending orbit

5.2 Post-processing phase

The numerical model produced a simulation of the expected subsidence induced at the surface by the collapse of voids created by the excavation of the two coal panels (W3 and W4). The model was produced along an N-S section crossing both the W3 and W4 panels (Fig. 5). To reproduce the chronology of the events and analyze if the differential exploitation of the two panels influenced the total measured subsidence, two calculation steps were performed. The first was related to the sole exploitation of the panel W4 (occurred from 2008 to 2010), whereas the second was related to the excavation of the W3 panel (which occurred from 2010 to 2012). Figure 7 shows that vertical displacements reach a maximum value of 32 cm. The lateral extent of the subsidence covers a horizontal length of about 1100 m, which is quite wider than the mined panel size. At the surface, the expected vertical displacement reaches a maximum value of 18 cm.

The availability of both ascending and descending datasets allowed us to reproduce the kinematics of the deformation through the displacement vector decomposition. The results, as shown in Figs. 8 and 9, are maps of vertical (VC) and horizontal (HC) components, with the total amount of displacement calculated in the time span 2011–2020. Considering an x, y, z Cartesian coordinate

system, HC maps coincide with the horizontal W-E and the VC maps with the vertical components. VC and HC were calculated considering three phases: pre-mining, syn-mining and post-mining activity. The availability of satellite dataset allowed to obtain one map during the pre-mining activity related to September 2011, where no displacement has been detected. During the W3 panel extraction carried out in the period 2011–2012 the displacement vector components were analyzed every two months. To understand the temporal evolution of displacements the progress of mining exploitation (i.e. the position of the exploitation front) has been integrated into the vector maps.

The post-mining activity was investigated every year from January 2013 onward. It is important to note that during the excavation of the W3 panel, between November 2011 and October 2012, only slight deformations can be identified. In detail, displacements started in November 2011 and developed until October 2012 with maximum cumulated vertical displacements of ca. 11 cm and horizontal ones between −14 cm and 4 cm. On the contrary, the largest deformations were detected in correspondence of post-mining operations, during the period from January 2013 to January 2014. Subsequently, subsidence continued slowly until January 2020 with maximum cumulated vertical displacements of ca. 26 cm and horizontal ones between −24 cm and 7 cm.
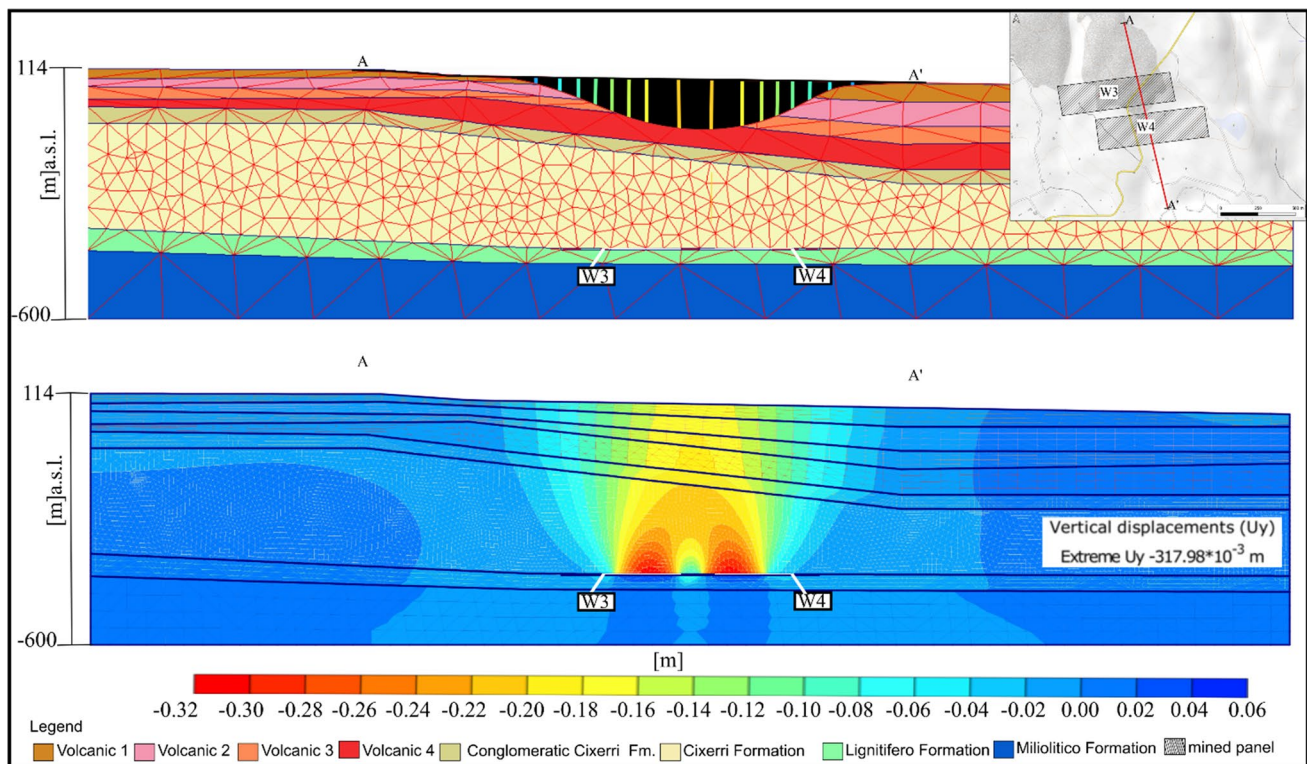

Fig. 7 Vertical displacements obtained by means of the geotechnical numerical model. On top subsidence profile related to the section *AA'*
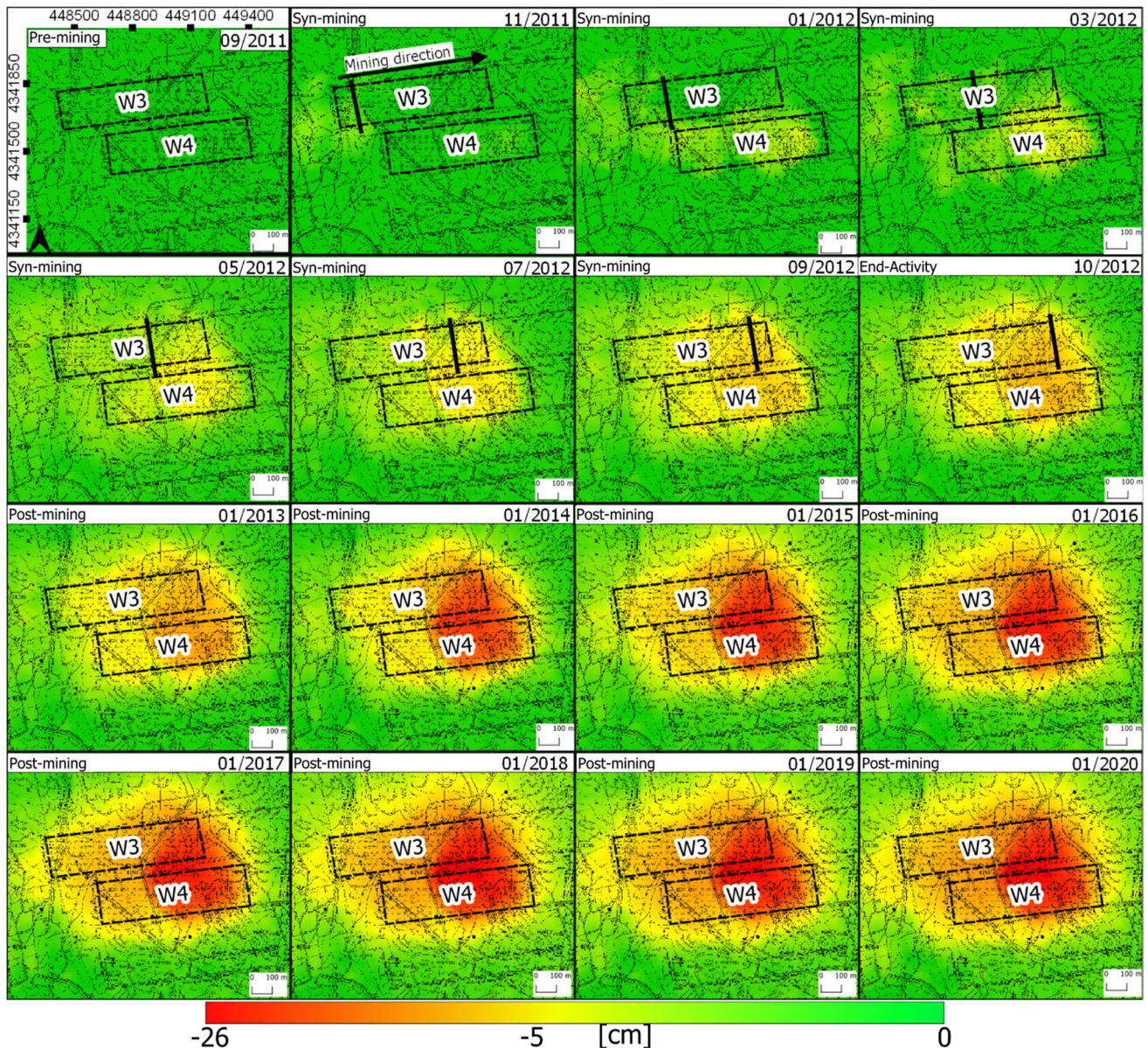
Fig. 8 Vertical deformation maps pre-mining, syn-mining, and post-mining activity. Black dashed lines in the figure represent the mining panels

6 Discussion

The aim of this work was to create a near-real time system for monitoring mining activity starting from PS-maps and using a subsurface3D geological model. The expected subsidence value was defined in the geotechnical numerical model of the rocks overlaying the two mining panels W4 and W3. Subsequently, the temporal vertical and horizontal component maps were created for monitoring the mining area during the exploitation and post-exploitation activity. Figure 10 shows the temporal evolution of vertical displacements along the N-S oriented profile cross-cutting the mined panels, compared with the expected subsidence along with

the same profile, as it was generated by the numerical model. The deformation started in November 2011, in correspondence with the W4 panel, and developed and extended until 2020, with maximum cumulated vertical displacements of ca. 26 cm located in the centre of two panels. It is important to note that most of the subsidence was temporally delayed respect to the coal exploitation.

In fact, during the mining activity, the expected subsidence was not exceeded, whereas the maximum deformation occurred during the post-mining operations. The delayed occurrence of the maximum deformation depends on several factors: peculiar features of the overburden geology, thickness of the panels, depth of the excavation area, and
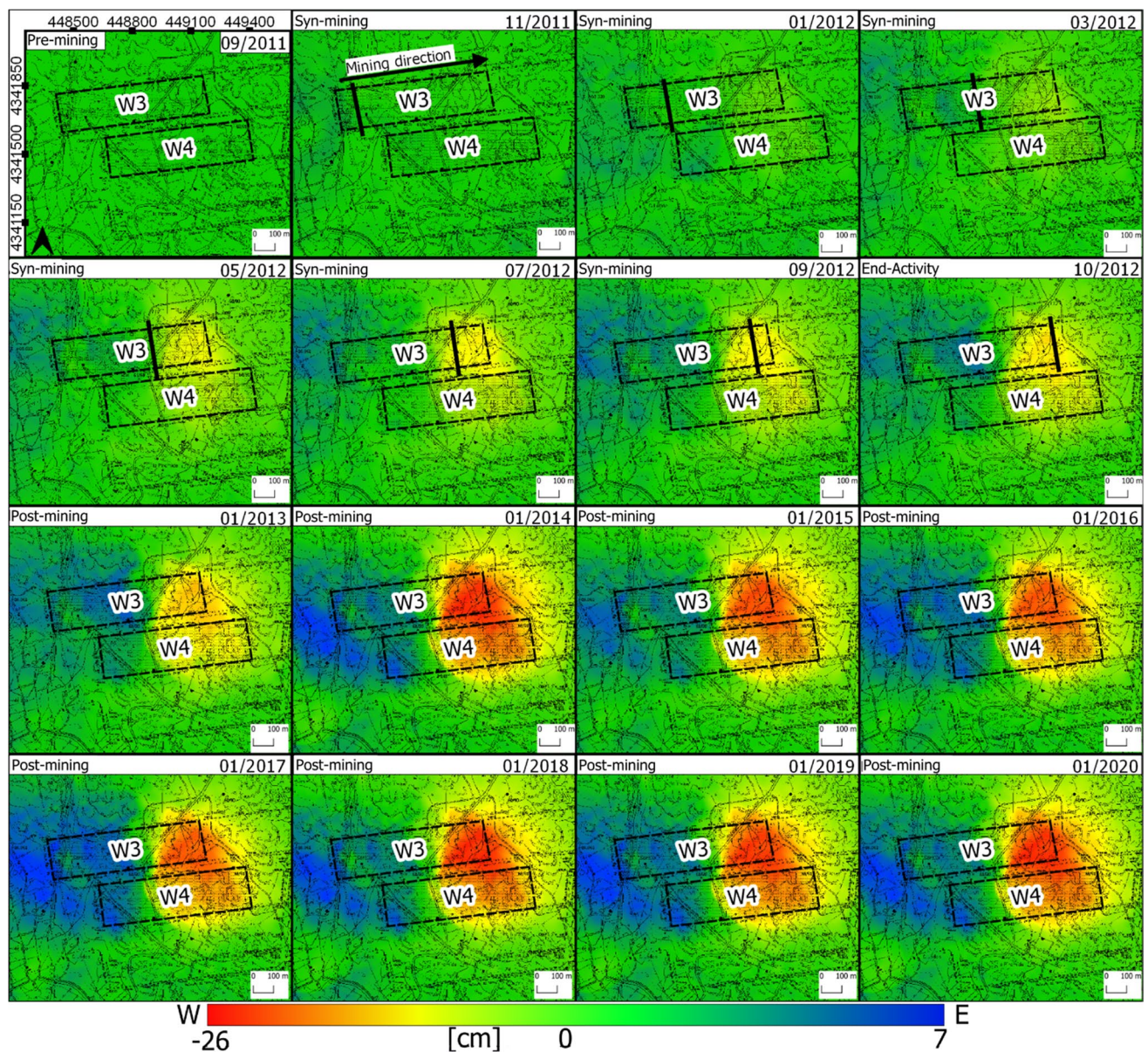
Fig. 9 Horizontal deformation maps pre-mining, syn-mining, and post-mining activity. Black dashed lines in the figure represent the mining panels

characteristics of the mining method. Several coal mining districts located in different countries, characterized by variable geological settings, show temporal delays in the occurrence of maximum surface deformations. This particular subsidence phenomenon, which is called residual subsidence (Alheib et al. 2005), continues after the extraction and in some cases can occur some months or years after the end of the underground mining activity (Huang et al. 2020; Cui et al. 2020; Modeste et al. 2021). Sometimes the residual surface deformation could be also characterized by uplift phenomena (Vervoort 2020). To understand the surface displacement, in Table 2 maximum horizontal (E-W direction)

and vertical components are compared with mining progress. During the extraction in 2011–2012, the major displacement reported showed a horizontal component (Fig. 9). This was likely due to the position of the new mined zone. Subsequently, it is possible to note that the vertical displacement increases respect to the horizontal one (Fig. 8). After the conclusion of mining activity, the deformation is concentrated between the two panels in the area characterized by the greatest geotechnical weakness (Table 2). This confirms that the observed displacements are directly related to the excavation process. The W3 panel was mined from 2011 to 2012 and the highest deformation increment was detected in
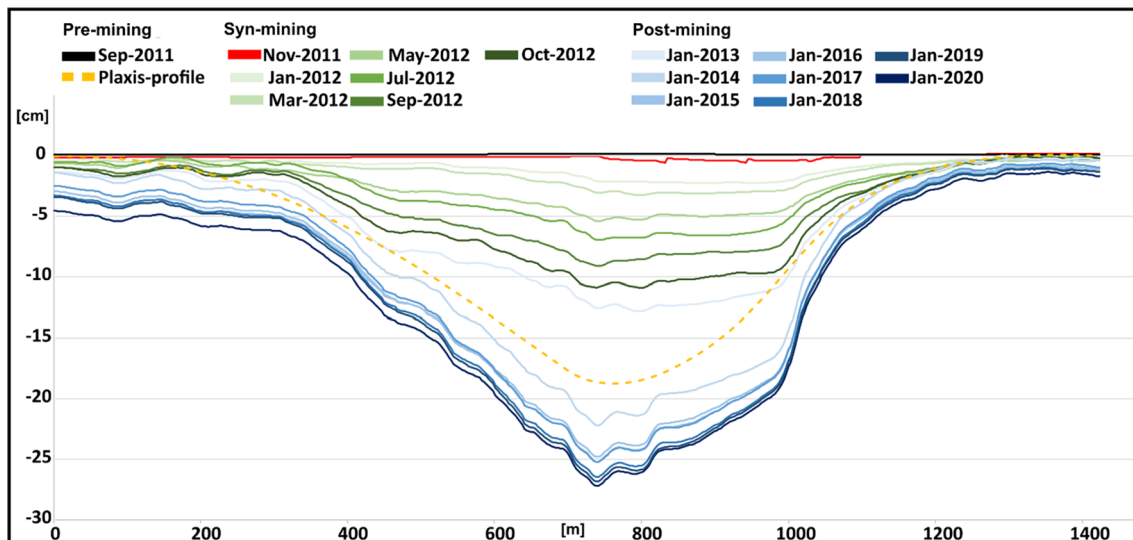
Fig. 10 Cumulated vertical deformation profiles during the pre-mining, syn-mining, and post-mining activity. Yellow dashed lines in the figure represent the expected subsidence

Table 2 Maximum vertical and horizontal displacements related to mining progress. the E-W and W-E were related to the directions of horizontal displacements

Date	Mining progress (m)	Vertical displacement max (cm)	Horizontal displacement max (E-W, cm)	Horizontal displacement max (W-E, cm)
Nov-11	95	− 1.00	− 1.40	1.00
Jan-12	102	− 2.60	− 3.20	1.90
Mar-12	160	− 3.30	− 5.80	3.00
May-12	120	− 5.40	− 9.60	3.50
Jul-12	118	− 6.80	− 10.70	3.70
Sep-12	78	− 8.90	− 10.40	4.22
Oct-12	37	− 11.25	− 14.50	4.33
Jan-13	–	− 13.00	− 14.48	5.32
Jan-14	–	− 22.21	− 19.21	6.15
Jan-15	–	− 24.80	− 22.30	5.29
Jan-16	–	− 25.18	− 21.50	6.70
Jan-17	–	− 25.20	− 21.20	7.50
Jan-18	–	− 26.20	− 24.60	6.00
Jan-19	–	− 26.30	− 23.48	7.37
Jan-20	–	− 26.40	− 24.30	7.23

January 2013, with differential vertical displacements of ca. 10 cm. In later times, the increment is of a few centimeters per year, with values decreasing with time until now.

According to several authors (Cui et al. 2000, 2020; Alheib et al. 2005; Tajduś et al. 2021), subsidence due to longwall mining is structured into three intervals. The first called initial subsidence, is the period when the surface movement lightly starts with low velocity.

The second phase (principal) is considered when displacements increase, generally up to 80% to 90% of final subsidence. The final phase, named "delayed" or

"residual" period, is associated with surface subsidence that continues after the end of mining activity, and can be characterized by 10% to 15% of final subsidence. This "delayed" period can start around 12–18 months, or also around 3–4 months after the end of the underground excavation, depending on the high or low geotechnical quality of the overburdened strata, respectively. In the Nuraxi-Figus study case, the second subsidence phase ends one year after the end extraction (Fig. 11), when the vertical displacement achieves about 84% of the final subsidence. The delayed subsidence starts in January 2015 and
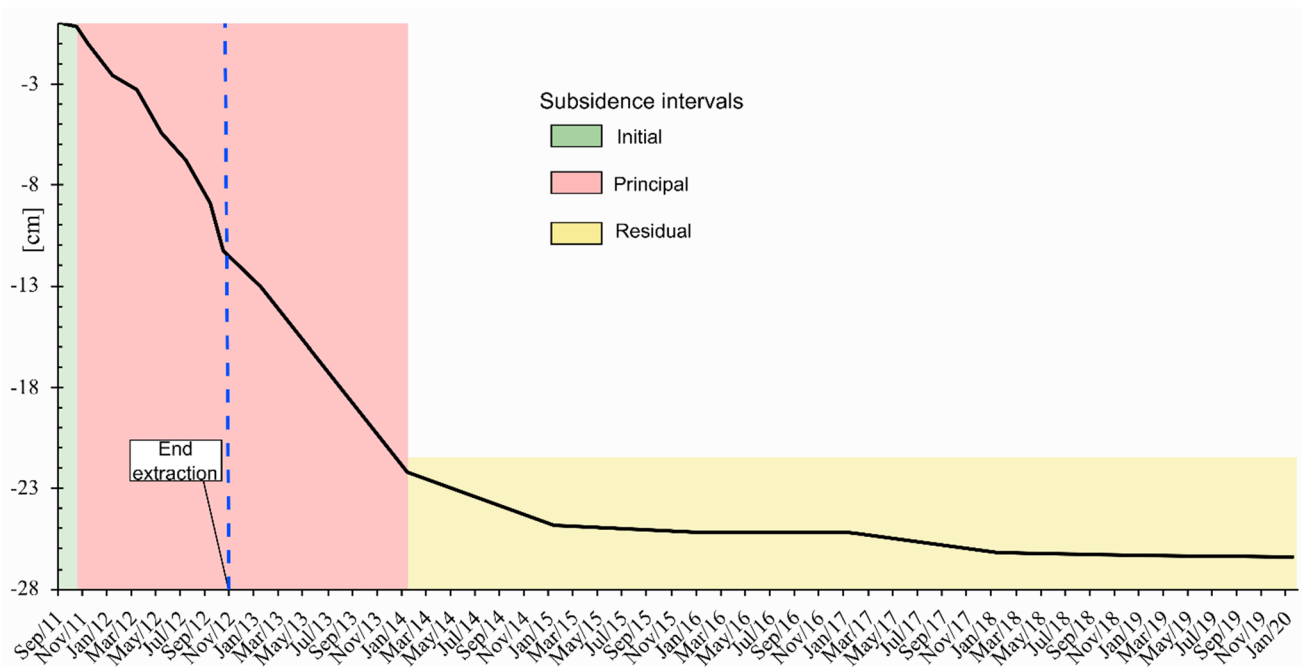
Fig. 11 Profile of maximum vertical cumulated displacement compared to three subsidence phases: initial (green), principal (red), residual (yellow)

develops slowly with a rate of about 20 mm/a (7% of final subsidence).

In the initial stages of underground mining, the caving zone is characterized by elastic deformations that recede if the overburdened forces are deleted. If extraction continues after a certain threshold, deformations become permanent. In this case, the pressure on the exploited areas increases, the sides move inward, the floor is subjected to uplift and the roof slides down (National Coal Board book 1965; Shadbolt et al.1978). According to Whittaker (1989), deformation occurring above a mining goaf depends on the following factors: depth of the cover, properties of overburden strata, seam thickness, geometry of the extraction panel, surficial topography, and extraction techniques. Specifically, in the underground mining four zones can be identified in the rock pile occurring above the extraction area. Starting from the bottom to the top there are: I—the zone immediately above the extraction area (caving zone), II—the fractured zone where the major cracks are present; III—the deformation zone, and IV—the surficial zone where subsidence could occur (Peng 1992). According to Mills (1998), the maximum subsidence (Sm) expected in an underground mining area is related to the width of the extraction panel (W), and height of cover strata (H). By using these parameters, it is possible to identify three types of excavation areas (Whittaker et al. 1989; Mills 2009):

(1) Supercritical (W/H > 1.6): Sm could be between 55% and 65% of the mined seam thickness;
(2) Critical W/H (from 0.6 to 1.6): Sm could be about 10% of the mined seam thickness, depending on changes in panel geometries, the overburden depth, and the composition and geotechnical properties of the strata;
(3) Subcritical (W/H < 0.6): Sm is negligible.

Applying the above subsidence model to the study area, it is possible to say that the caving zone should be completely included in the Lignitifero formation, whereas the fractured zone should affect the lower part of the Cixerri formation. The residual overlaying part of the Cixerri formation and the volcanic rocks should belong to the bending zone. In the geotechnical numerical model, it is possible to note that the maximum displacement is related to the Cixerri Formation. This is probably due to pre-existing structural discontinuities (fractures and faults), occurring in this Formation (Fadda et al. 1994), that were not considered in the geotechnical model. The surface zone is instead characterized by slight surface movements.

7 Conclusions

In this study, an integrated approach for near-real time mining monitoring was presented. The method allowed us to detect a subsidence phenomenon that occurred during the

mining activity and continued also for a few years after the completion of mining work. The study confirms that ground surface deformations can occur also in areas subjected to very deep underground mining and that the DinSAR techniques produce reliable results in terms of monitoring in a certain time span. The geotechnical numerical method can be used as subsidence forecasting model allowing to obtain the maximum expected amount of ground displacement. In underground mining areas, it is important to use monitoring techniques that can provide cost-effective regional perspectives for preventing possible negative environmental effects. The near real-time monitoring system applied in this study proved to be very useful for detecting subsidence during the mining activity and in the post-mining period. It is also important to emphasise that, in the absence of on-site monitoring, the method applied allowed us to reconstruct the phenomenon that occurred in order to undertake the necessary activities for the rehabilitation of the area. Therefore, it can be used for planning environmental remediation plans. However, to support the previous analysis and better investigate the subsidence-related cause-effect mechanism, as effectively as possible, it might be necessary to also acquire additional external data (i.e. leveling surveys, extensometers).

Declarations

Competing interest The authors declare no conflicts of interest.

References

Alheib M, Linkov AM, Zoubkov VV (2001) On numerical modeling of subsidence induced by mining. In International symposium of the international society for rock mechanics (EUROCK 2001)

Alheib M, Nicolas M, Noirel JF, Wojtkowiak F (2005) Residual subsidence analysis after the end of coal mine work. Example from Lorraine colliery, France

Alam MS, Kumar D, Chatterjee RS (2022) Improving the capability of integrated DInSAR and PSI approach for better detection, monitoring, and analysis of land surface deformation in underground mining environment. Geocarto Int 37(12):3607–3641

Ammirati L, Mondillo N, Rodas RA, Sellers C, Di Martire D (2020) Monitoring land surface deformation associated with gold artisanal mining in the Zaruma City (Ecuador). Remote Sens 12:2135

Ammirati L, Mondillo N, Calcaterra D, Di Martire D (2021) Sentinel-1 data for monitoring a pre-failure event of tailings dam. Lecture Notes in Civil Engineering 140–148

Armenakis C (1983) Subsidence determination by aerial photogrammetry. Geod Geomat Eng 93:1–118

Assorgia A, Cincotti F, Fadda A, Gimeno D, Morra V, Ottelli L, Secchi FA (1992a) Il complesso comenditico miocenico dell'entroterra sulcitano (Sardegna sud-occidentale) Caratteri geologici, vulcanologici e petrochimici. Boll Serv Geol It, Sp. Issue, pp 292–303

Assorgia A, Fadda A, Gimeno D, Morra V, Ottelli L, Pujolriu L, Secchi FA (1992b) Tectono-sedimentary evolution of the Upper Tertiary volcanic succession of Sulcis area (SW Sardinia, Italy). Paleontologia i Evolució 24–25:307–320

Barca S, Costamagna LG (2000) Il bacino paleogenico del Sulcis-Iglesiente (Sardegna SW): nuovi dati stratigrafico-strutturali per un modello geodinamico nell'ambito dell'orogenesi pirenaica. Boll Soc Geol It 119:497–515

Bell FG, Stacey TR, Genske DD (2000) Mining subsidence and its effect on the environment: some differing examples. Environ Geol 40(1):135–152

Bell FG, Donnelly LJ, Genske DD et al (2005) Unusual cases of mining subsidence from Great Britain, Germany and Colombia. Environ Geol 47:620–631

Bieniawski ZT (1989) Engineering rock mass classifications: a complete manual for engineers and geologists in mining, civil, and petroleum engineering. Wiley-Interscience. pp 40–47

Blanco P, Mallorquí JJ, Duque S, Monells D (2008) The coherent pixels technique (CPT): an advanced DInSAR technique for non-linear deformation monitoring. Pure Appl Geophys 165(6):1167–1193

National Coal Board (NCB). Subsidence engineer's handbook. NCB Mining Department; London, 1965 & 1975

Brinkgreve RBJ, Broere W, Waterman D (2008) Plaxis: finite element code for soil and rock analyses: 2D-version 8. User's manual

Carlà T, Farina P, Intrieri E, Ketizmen H, Casagli N (2018) Integration of ground-based radar and satellite InSAR data for the analysis of an unexpected slope failure in an open-pit mine. Eng Geol 235:39–52

Cascini L, Fornaro G, Peduto D (2010) Advanced low-and full-resolution DInSAR map generation for slow-moving landslide analysis at different scales. Eng Geol 112:29–42

Casu F, Bonano M, Castaldo R, De Luca C, De Novellis V, Lanari R, Zinno I (2019) Monitoring volcano deformation from space with Sentinel-1 Data for Civil Protection. In IGARSS 2019–2019 IEEE International Geoscience and Remote Sensing Symposium (pp 9303–9306). IEEE

Chen G, Cheng X, Chen W, Li X, Chen L (2014) GPS-based slope monitoring systems and their applications in transition mining from open-pit to underground. Int J Min Miner Eng 5(2):152–163

Chen B, Mei H, Li Z, Wang Z, Yu Y, Yu H (2021) Retrieving three-dimensional large surface displacements in coal mining areas by

combining SAR pixel offset measurements with an improved mining subsidence model. Remote Sens 13(13):2541

Colesanti C, Wasowski J (2006) Investigating landslides with space-borne Synthetic Aperture Radar (SAR) interferometry. Eng Geol 88:173–199

Costantini M, Ferretti A, Minati F, Falco S, Trillo F, Colombo D, Novali F, Malvarosa F, Mammone C, Vecchioli F, Rucci A, Fumagalli A, Allievi J, Ciminelli MG, Costabile S (2017) Analysis of surface deformations over the whole Italian territory by interferometric processing of ERS, Envisat and COSMO-SkyMed radar data. Remote Sens Environ 202:250–275

Costantini M, Falco S, Malvarosa F, Minati F (2008) A new method for identification and analysis of persistent scatterers in series of SAR images," In: Proc Int Geosci Remote Sensing Symp. (IGARSS), Boston MA, USA, 7–11 July 2008, pp 449–452

Cui X, Miao X, Wang J, Yang S, Liu H, Song Y, Liu H, Hu X (2000) Improved prediction of differential subsidence caused by underground mining. Int J Rock Mech Min Sci 37:615–627

Cui X, Zhao Y, Wang G, Zhang B, Li C (2020) Calculation of residual surface subsidence above abandoned longwall coal mining. Sustainability 12(4):1528

De Novellis V, Carlino S, Castaldo R, Tramelli A, De Luca C, Pino NA, Tizzani P (2018) The 21 August 2017 Ischia (Italy) earthquake source model inferred from seismological, GPS, and DInSAR measurements. Geophys Res Lett 45(5):2193–2202

Di Martire D, De Luca G, Ramondini M, Calcaterra D (2013) Landslide-related PS data interpretation by means of different techniques. In: Margottini C, Canuti P, Sassa K (eds) Landslide science and practice. Springer Berlin Heidelberg, pp 347–355

Di Martire D, Tessitore S, Brancato D, Ciminelli MG, Costabile S, Costantini M, Graziano GV, Minati F, Ramondini M, Calcaterra D (2016) Landslide detection integrated system (LaDIS) based on in-situ and satellite SAR interferometry measurements. Catena 137:406–421

Di Martire D, Paci M, Confuorto P, Costabile S, Guastaferro F, Verta A, Calcaterra D, (2017) A nation-wide system for landslide mapping and risk management in Italy: the second not-ordinary plan of environmental remote sensing. Int J Appl Earth Observ Geoinformation 63:143–157. https://doi.org/10.1016/j.jag.2017.07.018

Dong S, Yin H, Yao S, Zhang F (2013) Detecting surface subsidence in coal mining area based on DInSAR technique. J Earth Sci 24(3):449–456. https://doi.org/10.1007/s12583-013-0342-1

Du Z, Ge L, Li X, Ng AHM (2016) Subsidence monitoring over the Southern Coalfield, Australia using both L-Band and C-Band SAR time series analysis. Remote Sens 8:543

Fadda A, Ottelli L, Perna G (1994) Il Bacino lignitifero del Sulcis: Geologia, Idrogeologia, Miniere. Cagliari: Carbosulcis S.p.A

Foumelis M, Papageorgiou E, Stamatopoulos C (2016) Episodic ground deformation signals in Thessaly Plain (Greece) revealed by data mining of SAR interferometry time series. Int J Remote Sens 37(16):3696–3711

Franceschetti G, Migliaccio M, Riccio D, Schirinzi G (1992) Saras: a synthetic aper-ture radar (SAR) raw signal simulator. IEEE Trans Geosci Remote Sens 30:110–123

Gama FF, Paradella WR, Mura JC, de Oliveira CG (2019) Advanced DINSAR analysis on dam stability monitoring: a case study in the Germano mining complex (Mariana, Brazil) with SBAS and PSI techniques. Remote Sens Appl Soc Environ 16

Gazzola L, Ferronato M, Frigo M, Janna C, Teatini P, Zoccarato C, Antonelli M, Corradi A, Dacome MC, Mantica S (2021) A novel methodological approach for land subsidence prediction through data assimilation techniques. Comput Geosci 25(5):1731–1750

Giardina G, Milillo P, DeJong MJ, Perissin D, Milillo G (2019) Evaluation of InSAR monitoring data for post-tunnelling settlement damage assessment. Struct Control Health Monit 26(2)

Guerriero L, Confuorto P, Calcaterra D, Guadagno FM, Revellino P, Di Martire D (2019) PS-driven inventory of town-damaging landslides in the Benevento, Avellino and Salerno Provinces, southern Italy. J Maps 15(2):619–625

Guo H, Yuan L, Shen BT, Qu QD, Xue JH (2012) Mining-induced strata stress changes, fractures and gas flow dynamics in multi-seam long wall mining. Int J Rock Mech Min Sci 54:129–139

Holla L, Barclay E (2000) Mine Subsidence in the Southern Coalfield, NSW, Australia. Sydney, New South Wales Department of Mineral Resources

Huang C, Li Q, Tian S (2020) Research on prediction of residual deformation in goaf of steeply inclined extra–thick coal seam. PLoS ONE 15(10)

Iglesias R, Mallorqui JJ, Monells D, López-Martínez C, Fabregas X, Aguasca A, Gili JA, Corominas J (2015) PSI deformation map retrieval by means of temporal sublook coherence on reduced sets of SAR images. Remote Sens 7:530–563

Ismaya F, Donovan J (2012) Applications of DInSAR for Measuring mine-induced subsidence and constraining ground deformation model, GeoCongress 2012.

Ji M, Li X, Wu S, Gao Y, Ge L (2011) Use of SAR interferometry for monitoring illegal mining activities: a case study at Xishimen iron ore mine. Min Sci Technol (china) 21(6):781–786

Jing Z, Wang J, Zhu Y, Feng Y (2018) Effects of land subsidence resulted from coal mining on soil nutrient distributions in a loess area of China. J Clean Prod 177:350–361

Marschalko M, Yilmaz I, Bednárik M, Kubečka K, Bouchal T, Závada J (2012) Subsidence map of underground mining influence for urban planning: an example from the Czech Republic. Q J Eng GeolHydrogeol 45:231–241. https://doi.org/10.1144/1470-9236/11-048

Miano A, Mele A, Calcaterra D, Di Martire D, Infante D, Prota A, Ramondini M (2021) The use of satellite data to support the structural health monitoring in areas affected by slow-moving landslides: a potential application to reinforced concrete buildings. Struct Health Monit. https://doi.org/10.1177/1475921720983232

Milillo P, Giardina G, DeJong M, Perissin D, Milillo G (2018) Multi-temporal InSAR structural damage assessment: The London crossrail case study. Remote Sens 10:287

Mills KW, O'Grady P (1998) Impact of longwall width on overburden behaviour

Mills KW (2009) Subsidence engineering, Chapter 37. In Kininmouth, R. J and Baafi, E. Y (eds) Australasian Coal Mining Practice, 3 edition, Australasian Institute of Mining and Metallurgy, Monograph 12, pp 874−902

Modeste G, Doubre C, Masson F (2021) Time evolution of mining-related residual subsidence monitored over a 24-year period using InSAR in southern Alsace, France. Int J Appl Earth Obs Geoinf 102

Mora O, Mallorqui JJ, Broquetas A (2003) Linear and nonlinear terrain deformation maps from a reduced set of interferometric SAR images. Geosci Remote Sens 41:2243–2253

Morra V, Secchi FA, Assorgia A (1994) Petrogenetic significance of peralkaline rocks from Cenozoic calc-alkaline volcanism from SW Sardinia, Italy. Chem Geol 118(1–4):109–142

Necsoiu M, Walter GR (2015) Detection of uranium mill tailings settlement using satellite-based radar interferometry. Eng Geol 197:267–277

Pappalardo G, Mineo S, Angrisani AC, Di Martire D, Calcaterra D (2018) Combining field data with infrared thermography and

DInSAR surveys to evaluate the activity of landslides: the case study of Randazzo Landslide (NE Sicily). Landslides 15:1–21

Paradella WR, Ferretti A, Mura JC, Colombo D, Gama FF, Tamburini A, Santos AR, Novali F, Galo M, Camargo PO, Silva AQ, Silva GG, Silva A, Gomes LL (2015) Mapping surface deformation in open pit iron mines of Carajás Province (Amazon Region) using an integrated SAR analysis. Eng Geol 193:61–78

Pasci S, Carmignani L, Pisanu G, Sale V, Ulzega A, Orru P, Pintus C, Deiana G (2010) Note illustrative della carta geologica d'Italia -Foglio 564 Carbonia. Regione autonoma della Sardegna, 272 pp (in italian)

Pastor JL, Tomás R, Lettieri L, Riquelme A, Cano M, Infante D, Ramondini M, Di Martire D (2019) Multi-source data integration to investigate a deep-seated landslide Aecting a bridge. Remote Sens 11:1878

Pawluszek-Filipiak K, Borkowski A (2020) Integration of DInSAR and SBAS techniques to determine mining-related deformations using sentinel-1 data: the case study of Rydułtowy Mine in Poland. Remote Sens 12:242

Peng SS (1992) Surface subsidence engineering. Society for Mining, Metallurgy and Exploration, Littleton, Colorado

Prakash A, Lokhande RD, Singh KB (2010) Impact of rainfall on residual subsidence in old coal mine workings. J Environ Sci Eng 52(1):75–80

Przyłucka M, Herrera G, Graniczny M, Colombo D, Béjar-Pizarro M (2015) Combination of conventional and advanced DInSAR to monitor very fast mining subsidence with TerraSAR-X data: Bytom City (Poland). Remote Sens 7:5300–5328

Przyłucka M, Herrera G, Graniczny M, Colombo D, Béjar-Pizarro M (2015) Combination of conventional and advanced DInSAR to monitor fast mining subsidence with TerraSAR-X data: Bytom City (Poland). Remote Sens 7(5):5300–5328

Salmi EF, Nazem M, Karakus M (2017) The effect of rock mass gradual deterioration on the mechanism of post-mining subsidence over shallow abandoned coal mines. Int J Rock Mech Min Sci 91:59–71

Samsonov S, d'Oreye N, Smets B (2013) Ground deformation associated with post-mining activity at the French-German border revealed by novel InSAR time series method. Int J Appl Earth Obs Geoinf 23:142–154

Scifoni S, Bonano M, Marsella M, Sonnessa A, Tagliafierro V, Manunta M, Sciotti M (2016) On the joint exploitation of long-term DInSAR time series and geological information for the investigation of ground settlements in the town of Roma (Italy). Remote Sens Environ 182:113–127

Shadbolt CH (1978) Mining subsidence-historical review and state of the art, In: Geddes JD (eds) Conference on large ground movements and structures: Cardiff, Wales, 4–7, 1977, Proceedings, p 705–748

Singh KB, Singh TN (1998) Ground movement over longwall workings in the Kamptee coalfield, India. Eng Geol 50(1998):125–139

Tajduś K, Sroka A, Misa R, Hager S, Rusek J, Dudek M, Wollnik F (2021) Analysis of mining-induced delayed surface subsidence. Minerals 11:1187. https://doi.org/10.3390/min11111187

Tessitore S, Di Martire D, Mondillo N, Ammirati L, Boni M, Calcaterra D (2018) Detection of Subsidence by Radar Interferometric Data in the Seruci-Nuraxi Figus Coal Mine Area (Sardinia, Italy). IAEG/AEG Ann Meet Proc 3:51–55

Ullo SL, Addabbo P, Di Martire D, Sica S, Fiscante N, Cicala L, Angelino CV (2019) Application of DInSAR technique to high coherence sentinel-1 images for dam monitor-ing and result validation through in situ measurements. IEEE J Sel Top Appl Earth Obs Remote Sens 12:875–890

Vervoort A (2020) Long-term impact of coal mining on surface movement: Residual subsidence versus uplift. Min Rep Glückauf 156:136–141

Villegas T, Nordlund E, Dahner-Lindqvist C (2011) Hangingwall surface subsidence at the Kiirunavaara Mine, Sweden. Eng Geol 121:18–27

Vu KD, Nguyen TD, Dao NH, Duong TL, Dinh XV, Weber C (2021) Land subsidence induced by underground coal mining at Quang Ninh, Vietnam: persistent scatterer interferometric synthetic aperture radar observation using Sentinel-1 data. Int J Remote Sens 42(9):3563–3582

Wasowski J, Bovenga F (2022) Remote sensing of landslide motion with emphasis on satellite multi-temporal interferometry applications: an overview. Landslide Hazards, Risks, and Disasters, pp365–438

Whittaker BN, Reddish DJ (1989) Subsidence occurrence, prediction and control. Elsevier, Amsterdamn

Xie P, Luo Y, Wu Y, Gao X, Luo S, Zeng Y (2020) Roof deformation associated with mining of two panels in steeply dipping coal seam using subsurface subsidence prediction model and physical simulation experiment. Min Metall Explor 37(2):581–591

Xu X, Ma C, Lian D, Zhao D (2020) Inversion and analysis of mining subsidence by integrating DInSAR, offset tracking, and PIM Technology. J Sensors 2020:1–15

Ye S, Luo Y, Wu J, Yan X, Wang H, Jiao X, Teatini P (2016) Three-dimensional numerical modeling of land subsidence in Shanghai, China. Hydrogeol J 24(3):695–709

Yue H, Liu G, Guo H, Li X, Kang Z, Wang R, Zhong X (2011) Coal mining induced land subsidence monitoring using multiband spaceborne differential interferometric synthetic aperture radar data. J Appl Remote Sens 5(1)

Zhao X, Pan S, Sun Z, Guo H, Zhang L, Feng K (2021) Advances of satellite remote sensing technology in earthquake prediction. Nat Hazard Rev 22(1):03120001

Zhou DW, Wu K, Cheng GL et al (2015) Mechanism of mining subsidence in coal mining area with thick alluvium soil in China. Arab J Geosci 8:1855–1867

Zingano A, Weiss A (2019) Subsidence over room and pillar retreat mining in a low coal seam. Int J Min Sci Technol 29:51–57